Cellular Signalling 62 (2019) 109342

Contents lists available at ScienceDirect

Cellular Signalling

journal homepage: www.elsevier.com/locate/cellsig

Phosphodiesterase 3B (PDE3B) antagonizes the anti-angiogenic actions of PKA in human and murine endothelial cells

Jodi L. MacKeil[a], Paulina Brzezinska[a], Jonah Burke-Kleinman[a], Anne L. Theilmann[a,b], Christopher J.B. Nicol[c], Mark L. Ormiston[a,b], Donald H. Maurice[a,c,*]

[a] Department of Biomedical and Molecular Sciences, Queen's University, Kingston, ON K7L 3N6, Canada
[b] Department of Medicine, Queen's University, Kingston, ON K7L 3N6, Canada
[c] Department of Pathology and Molecular Medicine, Queen's University, Kingston, ON K7L 3N6, Canada

ARTICLE INFO

Keywords:
Endothelial cells
Sprouting angiogenesis
Protein kinase A
Phosphodiesterase 3B
cdc42

ABSTRACT

Recent reports show that protein kinase A (PKA), but not exchange protein activated by cAMP (EPAC), acts in a cell autonomous manner to constitutively reduce the angiogenic sprouting capacity of murine and human endothelial cells. Specificity in the cellular actions of individual cAMP-effectors can be achieved when a cyclic nucleotide phosphodiesterase (PDE) enzyme acts locally to control the "pool" of cAMP that activates the cAMP-effector. Here, we examined whether PDEs coordinate the actions of PKA during endothelial cell sprouting. Inhibiting each of the cAMP-hydrolyzing PDEs expressed in human endothelial cells revealed that phosphodiesterase 3 (PDE3) inhibition with cilostamide reduced angiogenic sprouting *in vitro*, while inhibitors of PDE2 and PDE4 family enzymes had no such effect. Identifying a critical role for PDE3B in the anti-angiogenic effects of cilostamide, silencing this PDE3 variant, but not PDE3A, markedly impaired sprouting. Importantly, using both *in vitro* and *ex vivo* models of angiogenesis, we show the hypo-sprouting phenotype induced by PDE3 inhibition or PDE3B silencing was reversed by PKA inhibition. Examination of the individual cellular events required for sprouting revealed that PDE3B and PKA each regulated angiogenic sprouting by controlling the invasive capacity of endothelial cells, more specifically, by regulating podosome rosette biogenesis and matrix degradation. In support of the idea that PDE3B acts to inhibit angiogenic sprouting by limiting PKA-mediated reductions in active cdc42, the effects of PDE3B and/or PKA on angiogenic sprouting were negated in cells with reduced cdc42 expression or activity. Since PDE3B and PKA were co-localized in a perinuclear region in human ECs, could be co-immunoprecipitated from lysates of these cells, and silencing PDE3B activated the perinuclear pool of PKA in these cells, we conclude that PDE3B-mediated hydrolysis of cAMP acts to limit the anti-angiogenic potential of PKA in ECs.

1. Introduction

Angiogenesis is a fundamental physiologic process for embryonic development and tissue repair in the adult [1]. The formation of new blood vessels is initiated when local tissue hypoxia promotes the release of pro-angiogenic stimuli, including vascular endothelial growth factor (VEGF). Upon it's release, VEGF activates quiescent endothelial cells (ECs) in nearby blood vessels and induces their differentiation into one of two highly specialized phenotypes. The first of these inducible phenotypes are referred to as endothelial "tip" cells, which direct vessel growth toward angiogenic signaling cues and anastomose with existing vascular structures to form an interconnected network [2–4]. Following these leader tip cells are proliferative "stalk" cells, which lengthen the newly developing blood vessel. Though angiogenesis is a critical adaptive response to hypoxia, dysregulated angiogenic activity contributes to a wide array of malignant, ischemic, and inflammatory disorders [5–8]. Given their role in directing new vessel growth, tip ECs serve as a preferential target for angiogenesis-related therapies. While the systems that regulate whether ECs adopt a tip or stalk phenotype are well defined [9–12], the mechanisms that allow tip cells to establish apical-basal polarity, generate filopodia to sense their environment, remodel and invade the extracellular matrix, and migrate toward pro-

Abbreviations: AC, Adenylyl cyclase; AKAR, A-kinase activity reporter; cdc42, Cell division control protein 42; EPAC, Exchange protein activated by cAMP; GEF, Guanine exchange factor; HAEC, Human arterial endothelial cell; MMP, Matrix metalloproteinases; PDE, Cyclic nucleotide phosphodiesterase; PKA, Protein kinase A; teloHAEC, Telomerase immortalized HAEC; VEGF, Vascular endothelial growth factor

* Corresponding author at: Department of Biomedical and Molecular Sciences, Queen's University, Kingston, ON K7L 3N6, Canada.
E-mail address: mauriced@queensu.ca (D.H. Maurice).

https://doi.org/10.1016/j.cellsig.2019.06.007
Received 3 May 2019; Received in revised form 3 June 2019; Accepted 4 June 2019
Available online 05 June 2019

angiogenic stimuli, are relatively poorly understood.

In ECs, the 3′,5′-cyclic adenosine monophosphate (cAMP) signaling system allows for spatial and temporal regulation of signals encoded by numerous hormones, neurotransmitters, cytokines and mechanical forces [13,14]. For instance, this ubiquitous second messenger system simultaneously regulates a myriad of EC functions, including maintenance of the endothelial permeability barrier [15,16] and the generation of new vascular structures [17–19], through its effectors, protein kinase A (PKA) and/or exchange protein activated by cAMP (EPAC). Ongoing studies in several laboratories, including ours, have established that spatial and temporal cAMP signaling is achieved, at least in part, when members of the multi-gene family of cyclic nucleotide phosphodiesterases (PDEs) co-localize with cAMP effector proteins and regulate local "pools" of cAMP [20,21]. Indeed, specificity in targeting individual cAMP effector-regulated functions has been achieved in model systems by targeting cAMP-signaling specifically within an individual macromolecular complex (*i.e.* cAMP-signalosome) rather than ubiquitously throughout all cellular cAMP signaling domains.

We recently reported that PKA, but not EPAC, acts in a cell autonomous fashion to constitutively reduce the angiogenic sprouting capacity of murine or human ECs by reducing levels of active cdc42, an effect which directly correlated with increased cdc42 binding to its negative regulator, GDIα [18]. While this recent work elucidated the underlying cellular and molecular mechanisms through which PKA regulates sprouting, it did not identify the PDE(s) that act to coordinate this specific action of PKA, nor did it report on whether PKA acted specifically by virtue of it being compartmented with a PDE in these cells. Here, we report that PDE3B specifically regulates the "pool" of cAMP through which PKA inhibits the intrinsic sprouting capacity of ECs. Using several model systems, including an *in vitro* spheroid model of sprouting angiogenesis and an *ex vivo* mouse retinal angiogenesis model, we show that pharmacological inhibition of PDE3 activity or PDE3B-silencing markedly impaired EC sprouting, an effect that correlates with increased PKA activity. At a cellular level, we show that PDE3B and PKA differentially regulate sprouting through several interdependent cellular events, including podosome rosette biogenesis, matrix degradation and, ultimately, cell invasion. At a molecular level, we demonstrate that PDE3B co-localizes with the PKA regulatory subunit, RIIβ, within a perinuclear domain and that these two proteins can be co-immunoprecipitated; in live cell FRET-based experiments, we show that PDE3B regulates PKA catalytic activity within this perinuclear domain. Lastly, we confirm that PDE3B regulates the anti-angiogenic effects of PKA in large part by effects downstream of cdc42. Collectively, these data identify PDE3B as a potential therapeutic target to manipulate angiogenesis.

2. Methods

2.1. Cell culture, siRNA transfection, stable cell lines

Human arterial (HA)ECs were cultured in VascuLife® VEGF media (LifeLine Cell Technology) at 37 °C in 5% CO_2. For siRNA transfection, cells were incubated with Lipofectamine 2000 (Invitrogen) and siRNA at a 1:1 ratio, as per manufacturer's instructions. Efficiency of RNAi-dependent knockdown was assessed *via* Western Blotting and/or polymerase chain reaction (qPCR), 48 h post-transfection. The following siRNA constructs were used: PKA(Cα) 5′-GGAAGCUCCCUUCAUACCAAAGUUU-3′, 5′-AAACUUUGGUAUGAAGGGAGCUUCC-3′ (Invitrogen); PDE3A 5′-GCUAUUUCUGCAGCUAACCAUGUA-3′ 5′-UUACAUGGUUAGCUGCAGAAAUAGC-3′ (Invitrogen); PDE3B 5′-GCCUCACCAAGAAUUUGGCAUUUCA-3′, 5′-UGAAAUGCCAAAUUCUUGGUGAGGC-3′ (Invitrogen); PDE3B SMARTpool 5′-CAGGAAGGAUUCUCAGUCA-3′, 5′-GUAAAGCUGAUGGGAAUAA-3′, 5′-GCGAAUUGCUUAUAUUUCU-3′, 5′-GGCAUAGAAUGGAGUAAUG-3′ (Dharmacon); cdc42 5′-UGAGAUAACUCACCACUGU-3′, 5′-ACAGUGGUGAGUUAUCUCA-3′ (Ambion); high GC universal negative control (Ambion).

For the generation of an AKAP-GR-expressing cell line, telomerase immortalized HAECs ("teloHAECs") were transfected with a plasmid encoding the A-kinase activity reporter (AKAR)-GR biosensor (a generous gift from Dr. Jin Zhang, UCSD) using TransfeX (ATCC) in accordance with manufacturer's instructions. To select for successfully transfected cells, teloHAECs were cultured in VascuLife® VEGF media supplemented with 250 μg/ml G418; following cell selection, teloHAECs expressing AKAR-GR were maintained in VascuLife® VEGF media with 125 μg/ml G418.

2.2. Spheroid angiogenesis assay

HAECs were trypsinized, resuspended in Vasculife® VEGF media containing 0.25% carboxymethylcellulose and experimental compounds, then plated in a 96-well round-bottom, non-adherent plate. Once the ECs had aggregated, multicellular spheroids were harvested and embedded in a type 1 collagen gel comprised of 3 vol of collagen stock solution (equilibrated to 2.0 mg/ml) with 1 vol EGM-2 containing 40% FBS, 1 vol 0.25% (*w/v*) methylcellulose, 25 ng/ml VEGF-A_{165} and experimental compounds The collagen-embedded spheroids were incubated at 37 °C with 5% CO_2 for 24 h to allow for VEGF-induced endothelial cell sprouting; live cell images were acquired with a Zeiss Axiovert S100 microscope equipped with a CCD camera. The total number of sprouts per spheroid were manually quantified from brightfield images. Experimental compounds utilized in the assay include: PKA inhibitor cocktail (PKAic; 1 μM H89, 1 μM mPKI, 1 μM KT5720, 200 μM cAMPs-RP), 30 μM 6-Bnz-cAMP, 100 nM Bay 60–7550, 5 μM cilostamide, 10 μM Ro20–1724, 10 μM ML141, and appropriate vehicles.

For mosaic spheroids, HAECs transfected with the relevant siRNA were labelled with either CellTracker™Green (RNAi-dependent knockdown) or CellTracker™Red (control siRNA); the differentially labelled HAECs were then trypsinized and combined in a 1:1 ratio. These mixed-cell suspensions were used to generate mosaic spheroids that were harvested and embedded in a collagen gel, as described above. Following 24 h of sprouting, live images of spheroids were acquired with a Zeiss Axiovert S100 microscope. Competition between the differentially labelled HAECs for the "tip" position in sprouts of each spheroid was measured and expressed as a percent of the total number of sprouts generated by the spheroid. In all experiments, a minimum of 10 spheroids were analyzed per condition and this was repeated in at least three independent experiments.

2.3. Chemotaxis and chemoinvasion assay

For chemotaxis studies, HAECs were trypsinized and plated in the upper chamber of a type 1 collagen-coated, (20 μg/ml) 8 μm porous FluoroBlok™ transwell insert (BD Biosciences); inserts were incubated for 2 h at 37 °C to allow cells to adhere to the upper surface of the porous membrane. Once cells adhered to the membrane, VEGF and FBS (10 ng/ml and 0.5%, respectively) were added to the bottom of the chamber to stimulate cell migration. Following a 4 h incubation period, transwell inserts were fixed with 4% paraformaldehyde, washed, permeabilized in 0.2% Triton X-100, blocked in 0.3% BSA, then stained with TRITC-conjugated phalloidin and DAPI to visualize F-actin and nuclei, respectively.

For chemoinvasion studies, HAECs were trypsinized, resuspended in a collagen gel (2 mg/ml), and plated in the upper chamber of an 8 μm porous FluoroBlok™ transwell insert (BD Biosciences). Inserts were incubated at 37 °C for 1 h on a flat, parafilm-covered surface to allow the collagen gel to polymerize. Once gelled, the inserts were transferred to a 24-well plate containing VEGF and FBS (50 ng/ml and 1%, respectively) to stimulate cell invasion through the polymerized collagen. After a 48 h incubation period, transwells were fixed and stained with TRITC-conjugated phalloidin and DAPI, as described previously. For

chemotaxis and chemoinvasion assays, whole cell migration and/or invasion to the bottom of the transwell insert were imaged with a Zeiss Axiovert S100 microscope and quantified using ImageJ software. To distinguish invasive activity from migratory functions, an invasive index was calculated from the ratio of invaded:migrated HAECs [22]. For chemotaxis and chemoinvasion studies, at least two experimental replicates were tested for a minimum of thee independent experiments.

2.4. Podosome studies

HAECs were plated on type 1 collagen-coated (20 μg/ml) coverslips and cultured in VascuLife® VEGF media supplemented with an additional 25 ng/ml VEGF and experimental compounds. After 24 h, cells were fixed in 4% paraformaldehyde, washed, permeabilized in 0.2% triton X-100, blocked in 0.3% BSA, then stained with an anti-cortactin antibody (#05–180, clone 4F11; Millipore), TRITC-conjugated phalloidin and DAPI. For high resolution images of podosomes and podosome rosettes, HAECs were imaged with a Leica TCS SP8 confocal laser scanning microscope. For quantification of podosome-positive and podosome rosette-positive HAECs, images were acquired with a Zeiss Axiovert S100 microscope. Individual podosomes were identified by the co-localization of cortactin and F-actin in 0.5-1 μm structures; podosome superstructures (*i.e.* rosettes) were identified as clusters of individual podosomes arranged in a ring-like structure (5-10 μm diameter) [23,24]. For quantification of the percent of HAECs expressing individual podosomes and/or podosome rosettes, at least 100 HAECs were analyzed per condition for a minimum of three independent experiments.

2.5. Collagen degradation assays

HAECs labelled with HOESCHT 33342 live cell nuclear stain were seeded on a MatTek glass bottom dish coated with a mix of type 1 collagen (20 μg/ml) and Fluorogenic DQ collagen (25 μg/ml). Once the cells adhered to the dish, HAECs were incubated with VEGF (25 ng/ml), or the vehicle, for 4 h, fixed in 4% paraformaldehyde, then imaged with a Zeiss Axiovert S100 microscope; imaging immediately following the fixation period was critical for optimized visualization of the fluorescent bi-products resulting from DQ-collagen degradation. Collagen hydrolysis was quantified by measuring the average fluorescence intensity per cell, for a minimum of 100 cells per condition, in at least three independent experiments.

2.6. Protein extraction, immunoprecipitation, and immunoblotting

HAECs were lysed in a triple detergent lysis buffer (1% Igepal, 10 mmol/L sodium pyrophosphate, 10 mmol/L sodium β-glycerophosphate, 5 mmol/L benzamidine,10 mM sodium orthovanadate, 50 mmol/L Tris-HCl, 150 mmol/L sodium chloride, 0.5% sodium deoxycholate, 0.1% SDS, 10 mmol/L sodium fluoride 0.1 mg/ml PMSF, 1 μg/ml pepstatin A, 1 μg/ml E-64, 5 μg/ml bestatin, 1 μg/ml aprotinin, 1 μg/ml leupeptin). For protein-protein interaction studies, cell lysates were precleared with protein A/G agarose and 1 μg/ml mouse IgG (4 h at 4 °C). Precleared HAEC lysates were incubated with either PDE3B antisera (ICOS Corporation) or mouse IgG (Santa Cruz) and protein A/G beads on a rotating platform for 16-24 h at 4 °C. Following this incubation, beads were collected by centrifugation and subsequently washed extensively with the lysis buffer. Proteins bound to the washed beads were eluted with 2× Laemmli buffer, resolved by SDS-page, electro-transferred to PVDF membranes (Millipore) and visualized by immunoblot analysis. For siRNA-mediated knockdown efficiency, 15-40 μg of HAEC lysate were analyzed by SDS-page and immunoblotting. Primary antibodies used for immunoblotting include: anti-PKAC (1 μg/ml; #485013, R&D Systems), anti-PDE3B (1 μg/ml; ICOS Corporation), anti-cdc42 (1:250; Cytoskeleton, #ACD03), and anti-β-actin (1:10000, Sigma-Aldrich, #A5441).

2.7. RNA isolation and qRT-PCR

HAEC or HMVEC RNA was isolated using a Qiagen RNeasy mini kit; RNA concentration and purity were measured using a NanoDrop 1000 (Thermo Fisher Scientific). cDNA was synthesized with a Qiagen Omniscript RT kit, as per manufacturer's instructions. For each qPCR reaction, PowerUp™ SYBR™ Green Master Mix (Thermo Fisher Scientific) was used with 10 ng cDNA template and the following primers: PDE3A (Fwd 5′-TTGGAGTTGATGGCGCTGTA-3′, Rev. 5′-CTGGCCGGGACDTGAAAAGA-3′), TBP (Fwd — 5′-TATAATCCCAAGCGGTTTGC-3′, Rev. — 5′-GCTGGAAAACCCAACTTCTG-3′), PGK (Fwd — 5′-CTGTGGGGGTATTTGAATGG-3′, Rev. — 5′-CTTCCAGGAGCTCCAAACTG-3′).

2.8. Fluorescence resonance energy transfer (FRET)

TeloHAECs stably expressing the AKAR-GR unimolecular sensor flanked by a GFP donor and mCherry as acceptor were used to measure PKA activity. Cells were plated on glass coverslips coated with type I collagen (20 μg/ml) and transferred to a dark room. The cells were mounted in a home-built flow perfusion chamber and perfused with modified Krebs buffer (25 mM NaCl, 5 mM KCl, 1 mM Na_2HPO_4, 1 mM $MgCl_2$, 5 mM dextrose, 20 mM HEPES, 2 mM $CaCl_2$, pH 7.40) and maintained at room temperature. Real-time FRET was performed using a Leica DMi8 inverted microscope equipped with a HC PL FLUOTAR 40×/1.30 oil immersion objective, a Leica EL6000 light source and a C11440 ORCA-Flash 4.0 digital camera (Hamamatsu). Resting baseline FRET measurements were captured over 5 min by perfusing the cells with Krebs buffer, followed by a 10 min perfusion with Krebs buffer supplemented with forskolin (10 μM) and IBMX (100 μM) to maximally saturate the sensor. FRET was quantified with three filter sets (CHROMA) as follows: for GFP, excitation filter 450/490 nm, DC 495 nm, emission 500/590 nm; for FRET (EGFP/mCherry), excitation 500/20 nm, DC 520 nm, emission 640 nm, for mCherry, excitation 532/558 nm, DC 565 nm, emission 570/640 nm. Images were acquired every 5 s with an exposure of 449 ms and processed using LAS X Version 2.0.0.14332 software (Leica). FRET changes were measured as changes in the background subtracted by the emission ratio of GFP over mCherry and correcting for bleed through of the emission of the donor into the acceptor channel and the bleed through of the acceptor emission into the donor channel. The resulting ratiometric traces are represented as the averaged traces of each condition to yield one single trace.

2.9. Ex vivo retina angiogenesis assay

Ai6(RCL-Zs green) mice [25] were crossed with a Cre-transgenic line, Tg(Alk1-cre)-L1 mice, resulting in GPF expression within the retinal endothelium. Isolation of retinas from postnatal day 5 mice was performed, as described previously [26]. Once harvested, retinas were embedded in type 1 collagen (2 mg/ml) containing experimental compounds (PKAic, 30 μM 6-Bnz-cAMP, 5 μM cilostamide, 10 μM ML141, or an appropriate vehicle). Embedded retinas were incubated for 7 h at 37 °C with 5% CO_2 and subsequently fixed with 4% paraformaldehyde overnight. Following several HBSS washes, retinas were flat mounted, and the retinal vasculature was imaged with a Zeiss Axiovert S100 microscope. Angiogenic activity in this *ex vivo* system was evaluated as by measuring the number of sprouts emerging from the front of the vascular plexus per field of view. All procedures were approved by the Queen's University Animal Care Committee in accordance with Canadian Council on Animal Care guidelines.

2.10. Cdc42 activation assay

Cdc42 activity pulldowns were performed using a Cdc42 activation kit (Cytoskeleton) in accordance with the manufacturer's protocol.

Briefly, HAECs were serum starved for 4 h, then treated with VEGF (25 ng/ml) and/or experimental compounds (PKAic, 5 μM cilostamide, or the vehicle) for 10 min. Following treatment, HAECs were washed with ice-cold HBSS, then lysed in a Tris-based lysis buffer. Active (GTP-bound) cdc42 was isolated from the lysates using GST-p21 activated kinase p21 binding domain (PAK-PBD) beads. The pulldowns were resolved by SDS-page and analyzed by immunoblot.

2.11. Statistics

Statistical analysis was performed using GraphPad Prism 8 software. All graphs are presented as the means ± standard error of the mean (SEM). The D'Agostino and Pearson test was used to assess the normality of distribution of investigated parameters. For normal data, a student's unpaired *t*-test was used to determine significance between two groups, and a one-way ANOVA was used for data sets with greater than two groups. For non-normal data, statistical analysis for two groups was conducted with a Mann-Whitney *U* test, and greater than two groups with a Kruskal-Wallis and Dunn's test. Values were considered statistically significant at $p \leq 0.05$. Unless otherwise stated, all data were collected in a minimum of three independent experiments.

3. Results

3.1. PKA and PDE3B differentially regulate human arterial EC sprouting angiogenesis

Recent reports have identified PKA as a negative regulator of angiogenic sprouting [17,18]. Given that cAMP-effector selectivity in cells can be regulated by their co-localization with PDE(s) [14,20,21], we sought to explore whether cAMP-hydrolyzing PDE(s) regulate PKA activity in the context of angiogenic sprouting. To elucidate which of the cAMP-dependent PDEs predominantly expressed in ECs, namely PDE2, PDE3 and PDE4 [20,27], influence sprouting, we selectively inhibited each enzyme and assessed the impact of these treatment on sprouting in an *in vitro* spheroid model. While inhibition of PDE2 with Bay 60–7550 had no impact on HAEC sprouting relative to controls, treatment of EC spheroids with cilostamide, a PDE3 inhibitor, significantly impaired angiogenic sprouting (Fig. 1a, b). Of note, the observed decrease in sprouting was indistinguishable from that seen when spheroids were treated with a PKA-selective activator, 6-Bnz-cAMP, implicating PDE3 family of enzymes as a potential regulator of PKA activity during sprouting. In marked contrast, spheroids treated with the PDE4 inhibitor, Ro20–1724, exhibited a hyper-sprouting phenotype similar to that of spheroids treated with a PKA inhibitor cocktail (Fig. 1a, b), an effect inconsistent with a role for this PDE in regulating the ability of PKA to inhibit sprouting. Taken together, these data indicate that distinct PDE families, specifically PDE3 and PDE4, have opposing roles in the regulation of EC sprouting. Furthermore, these results suggest that PDE3 may function as a potential regulator of PKA activity, given that inhibition of this cAMP-hydrolyzing enzyme mirrored the effects of PKA activation.

Since HAECs express enzymes encoded by each of the two known PDE3 genes, namely *PDE3A* and *PDE3B* [27], and both PDE3A and PDE3B activities are efficiently inhibited by cilostamide [28], our findings were silent with respect to the "relative" involvement of these two PDE3 isoforms in regulating sprouting. To determine whether cilostamide-mediated inhibition of sprouting was due to changes in total PDE3 activity, or more selectively due to inhibition of one of these PDE3 variants, we next investigated the roles of PDE3A and PDE3B during angiogenic sprouting using the competitive mosaic spheroid model. In this system, cells with reduced levels of the gene of interest (*i.e.* PKA(Cα), PDE3A, or PDE3B) must compete with neighbouring control cells for the "tip position" in newly forming angiogenic sprouts; knockdown efficiency for each gene was validated at the protein (Fig. 1g, m) or mRNA level (Fig. 1j). To identify distinct populations within the mosaic spheroid, HAECs were either labelled with CellTracker™ Green or Red; importantly, the differentially labelled cells show no preference for tip cell occupancy (Fig. 1c,d). Consistent with our previous works [18], HAECs with reduced expression of PKA(Cα) exhibited an enhanced sprouting capacity, as demonstrated by their dominance in tip cell occupancy (≥80%) (Fig. 1e, f). Although PDE3A-silenced HAECs did show a modest, albeit significant, decrease in their ability to occupy the tip position (Fig. 1h, i), the ability of PDE3B-silenced HAECs to compete with HAEC controls for tip cell occupancy was drastically reduced. Indeed, silencing PDE3B with either of two distinct siRNAs markedly impaired endothelial cell sprouting, with fewer than 25% of PDE3B-knockdown cells establishing the tip position in newly forming sprouts (Fig. 1k, l; PDE3B SMARTpool siRNA data not shown). Given the subtle effect of PDE3A-knockdown on EC sprouting compared to the marked effects of PDE3B-knockdown, our data are consistent with the conclusion that the effects of cilostamide were largely mediated through PDE3B inhibition. Furthermore, the opposing effects of PKA(Cα)- and PDE3B-knockdown in the mosaic spheroid model are consistent with the hypothesis that PDE3B regulates PKA activity during angiogenic sprouting.

3.1.1. Silencing HAEC PDE3B reduces their migration, invasion, podosome rosette formation and collagen matrix degradation

Tip cell sprouting in response to a pro-angiogenic stimulus requires a myriad of highly coordinated cellular events. We previously reported that PKA regulates angiogenic sprouting by restricting podosome rosette biogenesis, MMP-dependent matrix degradation, and cell invasion [18]. Since our *in vitro* angiogenesis studies provided compelling evidence for PDE3B regulation of PKA during sprouting, we next investigated the underlying cellular mechanisms through which PDE3B regulates EC sprouting. To this end, we used a modified Boyden chamber assay to assess the impact of silencing PKA(Cα) or PDE3B on HAEC chemotaxis and chemoinvasion. Consistent with our previous studies [18], silencing PKA(Cα) promoted HAEC invasion (Fig. 2a, c, d), but had no impact on cell migration in response to a chemotactic stimulus (Fig. 2a, b). On the other hand, cells with reduced expression of PDE3B exhibited both hypo-migratory (Fig. 2a, b) as well as hypo-invasive (Fig. 2a, c) phenotypes when compared to control HAECs. Importantly, the invasive index of PDE3B-knockdown cells was significantly lower than that of controls (Fig. 2d), indicating that the hypo-invasive phenotype observed in these cells is not simply a reflection of their reduced migratory capacity.

EC invasion is associated with the generation of podosomes, submicron (0.5-1 μm) actin-rich structures that recruit and activate matrix metalloproteinases (MMPs) to allow for focal matrix degradation. Although podosomes may exist as individual entities, in many cell types, including HAECs, they can also form larger superstructures (5-10 μm) termed podosome rosettes. Importantly, several studies have demonstrated that the generation of podosome rosettes precedes vascular sprouting [23,29]. Given that sprouting and invasion were both impaired in PDE3B-silenced HAECs, we suspected that these cells may have a reduced capacity to generate podosomes and/or podosome rosettes. To test this hypothesis, we assessed the percent of PKA(Cα)- and PDE3B-silenced HAECs that expressed individual podosome or podosome rosettes following a 24 h treatment with the pro-angiogenic agent, VEGF. While silencing PKA(Cα) increased the number of HAECs expressing either individual podosomes or podosome rosettes (Fig. 2e-g), PDE3B-knockdown markedly decreased the number of HAECs expressing the podosome rosette superstructures (Fig. 2e, g).

To investigate the functional impact of reduced podosome rosette expression in PDE3B-knockdown cells, we assessed their ability to degrade the extracellular matrix using fluorogenic DQ™ collagen model. In this system, proteolytic activity is measured by the emission of a green fluorescence signal following DQ™ collagen hydrolysis. Though stimulating control HAECs with VEGF (25 ng/ml) significantly increased collagen hydrolysis compared to cells cultured under basal

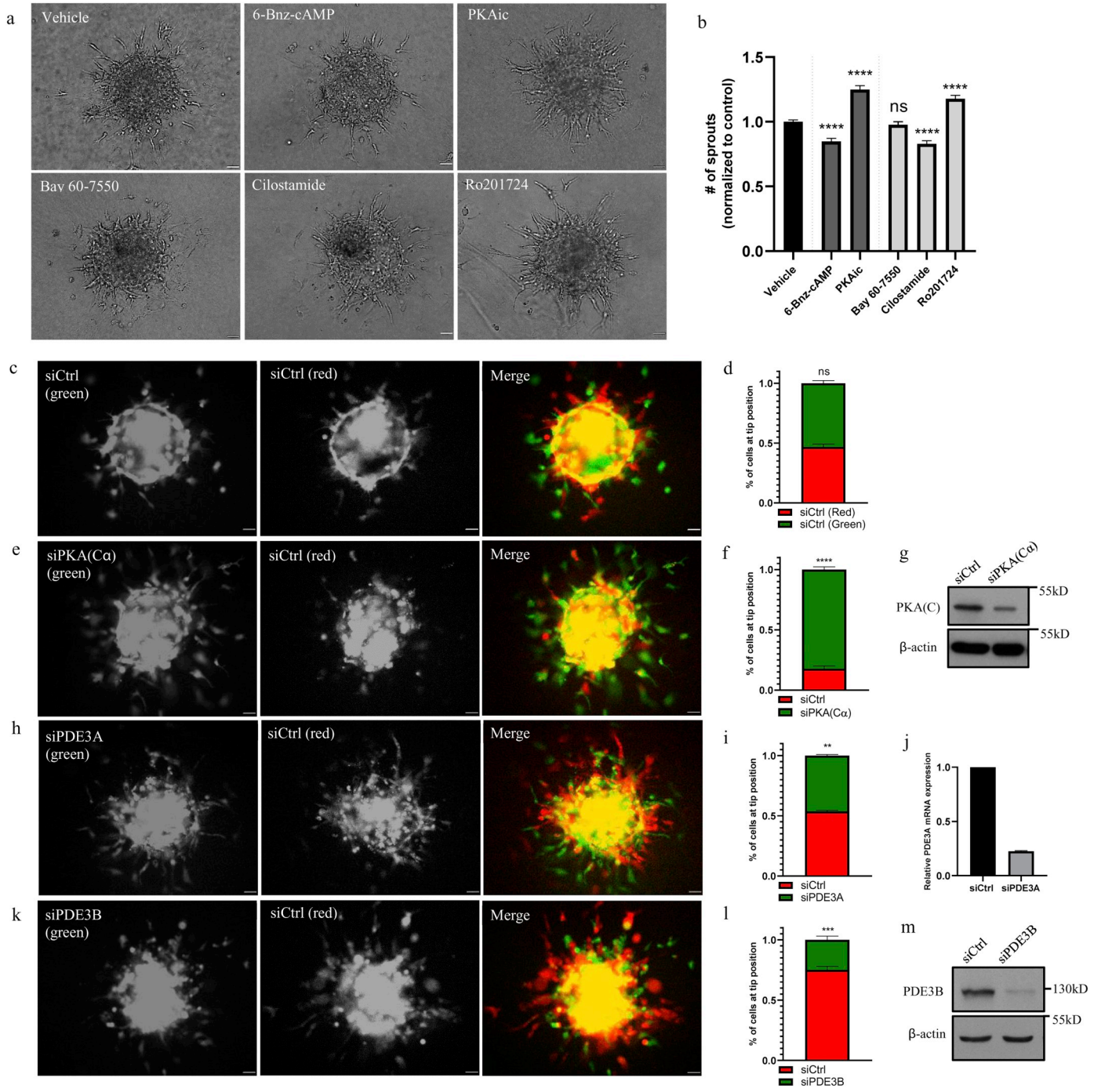

Fig. 1. PKA and PDE3B differentially regulate angiogenic sprouting *in vitro.* (a) Representative brightfield images of HAEC spheroids treated with a PKAic (1 μM H89, 1 μM mPKI, 1 μM KT5720, 200 μM cAMPs-RP), 6-Bnz-cAMP (30 μM), Bay 60–7550 (100 nM), cilostamide (5 μM), Ro20–1724 (10 μM) or the vehicle; scale bars, 50 μm. (b) Quantitation of HAEC sprouting ($n = 3$; $^{****}p < 0.0001$ in one-way ANOVA). (c, e, h, k) Representative images of the competitive sprouting angiogenesis assay. Mosaic spheroids were generated from a 1:1 mixture of (c) siCtrl-siCtrl, (e) siCtrl-siPKA(Cα), (h) siCtrl-siPDE3A, or (k) siCtrl-siPDE3B HAECs. EC identity in sprouting spheroids was determined by differentially labelling ECs with CellTracker™ Green, or CellTracker™. Scale bars, 50 μm. (d, f, i, l) The competitive sprouting was assessed by quantifying tip cell occupancy of CellTracker™ Green- or CellTracker™ Red-labelled cells in individual HAEC spheroids. Values are expressed as a percentage of the total number of sprouts formed in each spheroid (n = 3; $^{***}p < 0.001$, $^{****}p < 0.0001$ in Student's unpaired *t*-test). (g, m) Representative immunoblots of PKA(Cα) and PDE3B knockdown efficiency (n = 3). (j) Relative mRNA expression demonstrating PDE3A knockdown efficiency ($n = 2$). (For interpretation of the references to colour in this figure legend, the reader is referred to the web version of this article.)

conditions, the effect of the pro-angiogenic stimulus was blunted in HAECs with reduced PDE3B levels (Fig. 2h,i). Furthermore, matrix degradation by PDE3B-knockdown HAECs was drastically reduced compared to controls, both under basal conditions and following VEGF stimulation (Fig. 2h,i). Collectively these data support the idea that impaired angiogenic sprouting following PDE3B-knockdown and/or inhibition with cilostamide is attributed to a decrease in the presence of podosome rosettes, reduced matrix degradation and a diminished invasive capacity. Perhaps more importantly, the opposing effects of PKA(Cα)- and PDE3B-knockdown on HAEC invasion, podosome rosette biogenesis, matrix degradation and sprouting provide further evidence that PDE3B selectively controls the effects of PKA on EC sprouting.

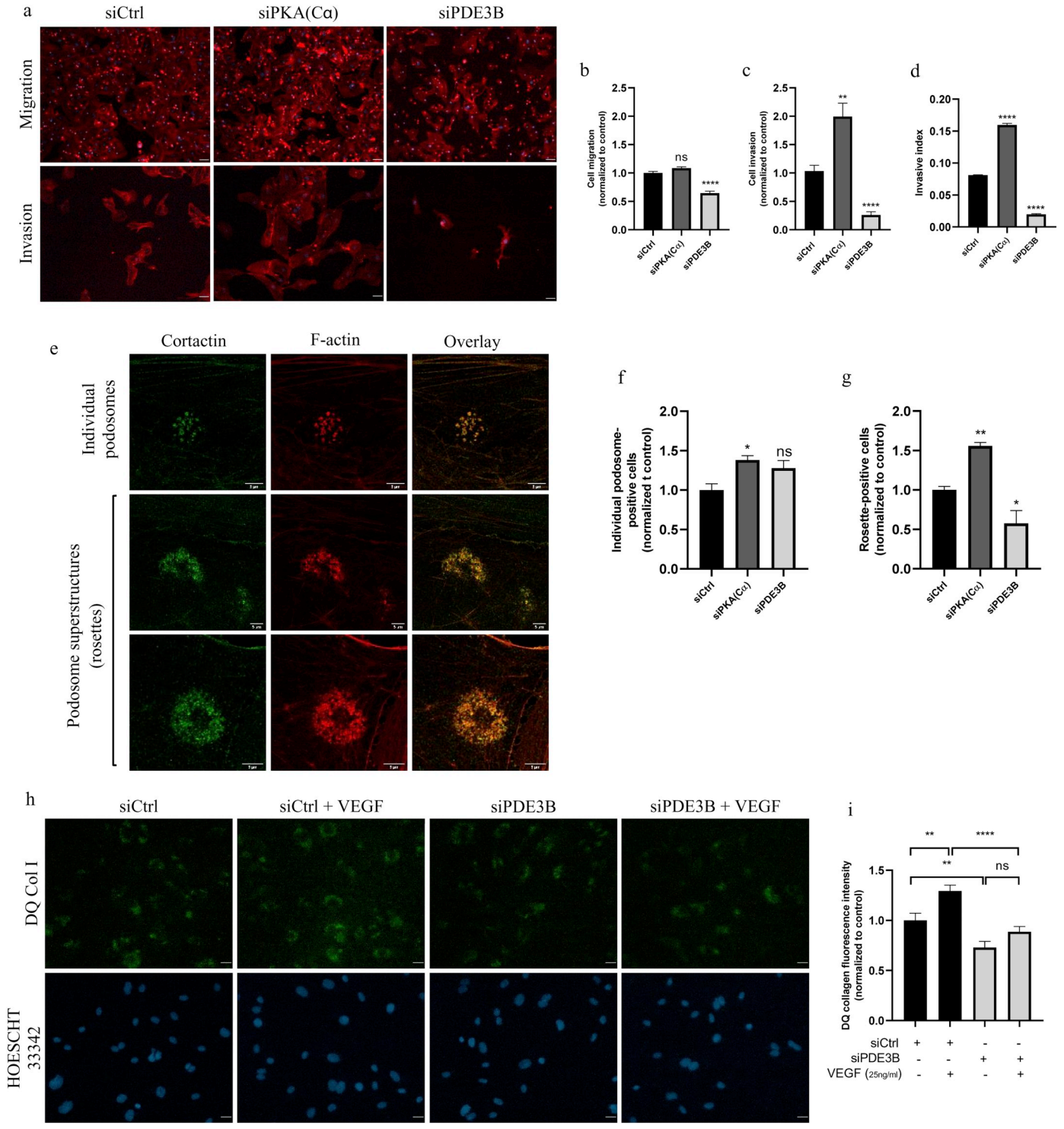

Fig. 2. Selective knockdown of PDE3B impairs endothelial cell invasion, podosome rosette formation, and matrix degradation. (a) Representative images of the chemotaxis and chemoinvasion assays. F-actin and nuclei from migrating and/or invading cells were visualized with TRITC-conjugated phalloidin and with DAPI, respectively; scale bars, 50 μm. (b-d) Quantification of whole cell (b) chemotaxis, (c) chemoinvasion, (d) and the invasive index of siCtrl, siPKA(Cα), and siPDE3B HAECs. The invasive index was calculated as the ratio of invaded:migrated endothelial cells. (b, d) ****p < 0.0001 with one-way ANOVA, (c) **$p < 0.01$, ****p < 0.0001 in Kruskal-Wallis test. (e) Representative confocal images of individual podosomes and podosome superstructures (i.e. rosettes) in HAECs; scale bars 5 μm. (f, g) Quantitation of the percent of ECs expressing (f) individual podosomes and/or (g) podosome rosettes following 24 h treatment with VEGF (25 ng/ml); *$p < 0.05$, **$p < 001$ in one-way ANOVA. (h) Representative images of showing DQ-Col-I degradation (green) by HOESCHT33342-labelled HAECs (blue) under basal conditions or following stimulation with an additional 25 ng/ml VEGF. (i) Quantitation of DQ-collagen degradation, measured as the average FITC fluorescence intensity per cell (n = 3, **p < 0.01, ****p < 0.0001 in one-way ANOVA). (For interpretation of the references to colour in this figure legend, the reader is referred to the web version of this article.)

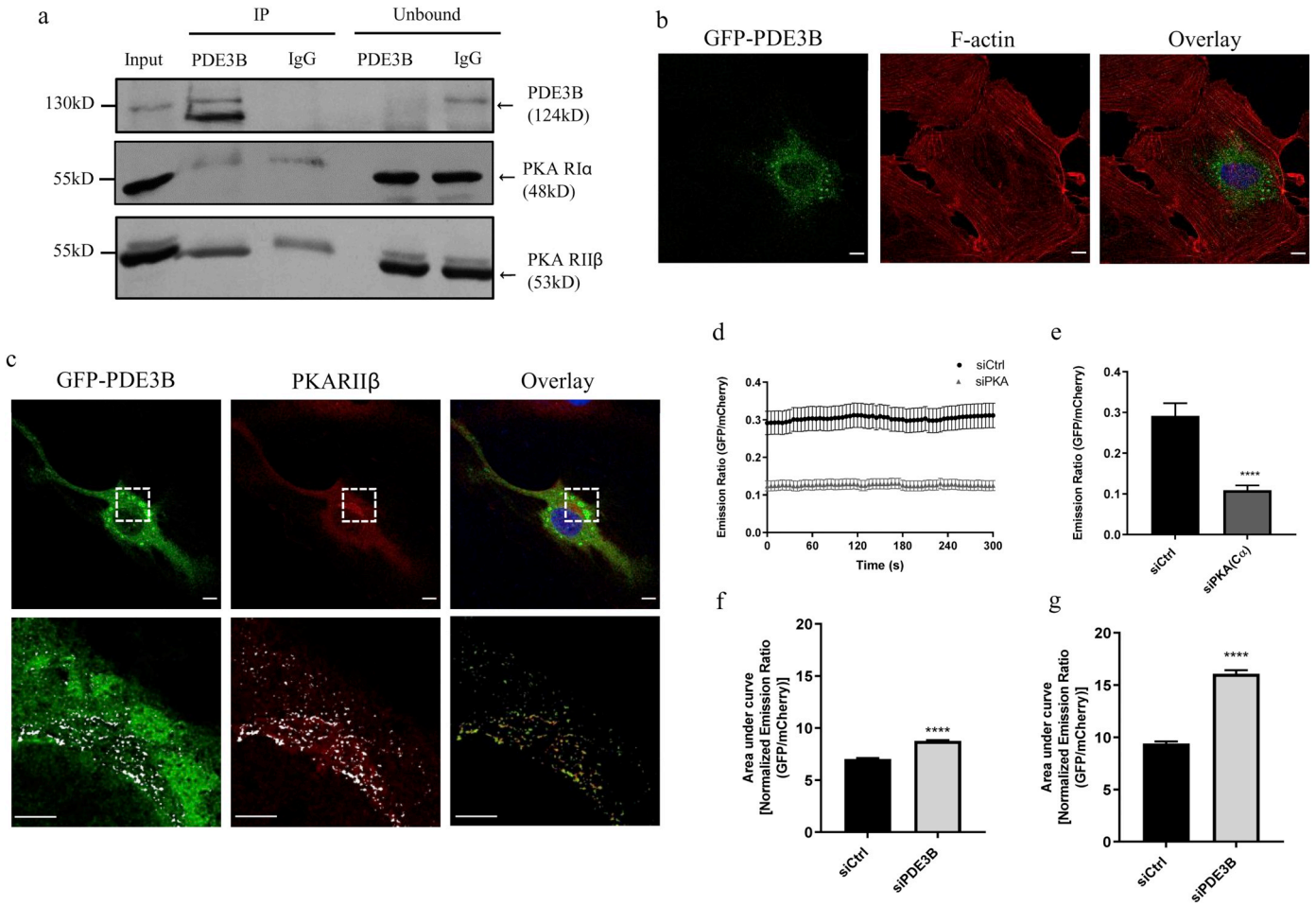

Fig. 3. PDE3B tethers PKA and regulates its catalytic activity. (a) Representative immunoblot showing direct interaction of endogenous PDE3B and PKARIIβ. HAEC lysates were subjected to anti-PDE3B immunoprecipitation; isolated protein complexes were resolved by SDS page and immunoblotted for endogenous PKARIα, PKARIIβ, and PDE3B. (b) Representative high-resolution confocal images showing GFP-tagged PDE3B localization in the perinuclear region of the HAECs. Scale bars denote 50 μm. (c) Representative high-resolution confocal images showing PKARIIβ co-localization with GFP-tagged PDE3B in the perinuclear region of HAECs. Scale bars in top panel, 50 μm; scale bars in bottom panel, 5 μm. (d) Plot of average PKA activity in control- and PKA(C)-knockdown teloHAECs stably expressing the AKAR-GR FRET biosensor at baseline, for $n = 13$ cells. (e) Quantification of the FRET emission ratio in control- and PKA(C)-knockdown teloHAECs. (f, g) Quantification of the normalized FRET emission ratio for the (f) whole cell and (g) perinuclear region of control ($n = 21$ cells) and PDE3B-KD teloHAEC ($n = 34$ cells) stably expressing AKAR-GR; ****$p < 0.0001$ in Student's unpaired t-test.

3.2. PDE3B associates with PKA and regulates its catalytic activity in HAECs

Since PKA and PDE3B differentially regulate podosome rosette biogenesis, cell invasion and angiogenic sprouting, we next chose to confirm our earlier finding that PDE3B and PKA integrate into a cAMP-signaling complex in HAECs [30]. As predicted, immunoprecipitation of endogenous HAEC PDE3B allowed recovery of the PKA regulatory subunit, PKA-RIIβ (Fig. 3a). Interestingly, immunoblot analysis was inconsistent with interactions between PDE3B and another PKA regulatory subunit, namely PKA-RIα (Fig. 3a). In addition, immunofluorescence imaging verified co-localization of endogenous PKARIIβ with a GFP-tagged PDE3B within the perinuclear region of HAECs (Fig. 3b, c); regrettably, the PDE3B antibody used for our immunofluorescence studies did not have a sufficiently avidity to allow detection of endogenous levels of PDE3B in these cells. To explore the functional impact of PDE3B-PKA co-localization in HAECs, we measured the impact of silencing PDE3B on PKA activity in a stable HAEC line expressing the PKA activity biosensor, AKAR-GR [31]. Validating our approach, PKA(Cα)-knockdown significantly reduced global PKA activity in these cells, as measured by a decrease in the FRET emission ratio (Fig. 3d, e). Although silencing PDE3B resulted in a small, albeit significant, increase in total cellular PKA activity (Fig. 3f), it drastically increased PKA activity within the perinuclear region (Fig. 3g) where PDE3B is highly localized (Fig. 3b). Taken together, these data identify a role for PDE3B in regulating a perinuclear "pool" of PKA in HAECs.

3.3. PKA inhibition reverses the hypo-sprouting phenotype induced by cilostamide or PDE3B-silencing

To determine if PDE3B regulation of PKA activity was relevant during vascular sprouting, we used an *in vitro* spheroid model of angiogenesis to assess whether PKA inhibition could rescue the hypo-sprouting phenotype induced by PDE3B-knockdown. In support of a role for a PDE3B-PKA signaling axis in regulating EC angiogenesis, inhibiting PKA activity in PDE3B-silenced spheroids resulted in a significant increase in HAEC sprouting (Fig. 4a, b). Given that silencing PDE3B influenced both the invasive and the migratory capacities of these cells, while PKA only regulated their invasive capacity, we did not anticipate that PKA inhibition would fully restore endothelial cell sprouting in PDE3B-silenced spheroids. To confirm that the restorative effects of PKA inhibition were associated with an enhanced invasive capacity in these cells, we next studied whether PKA inhibition could rescue the appearance of podosome rosettes in cells with reduced levels

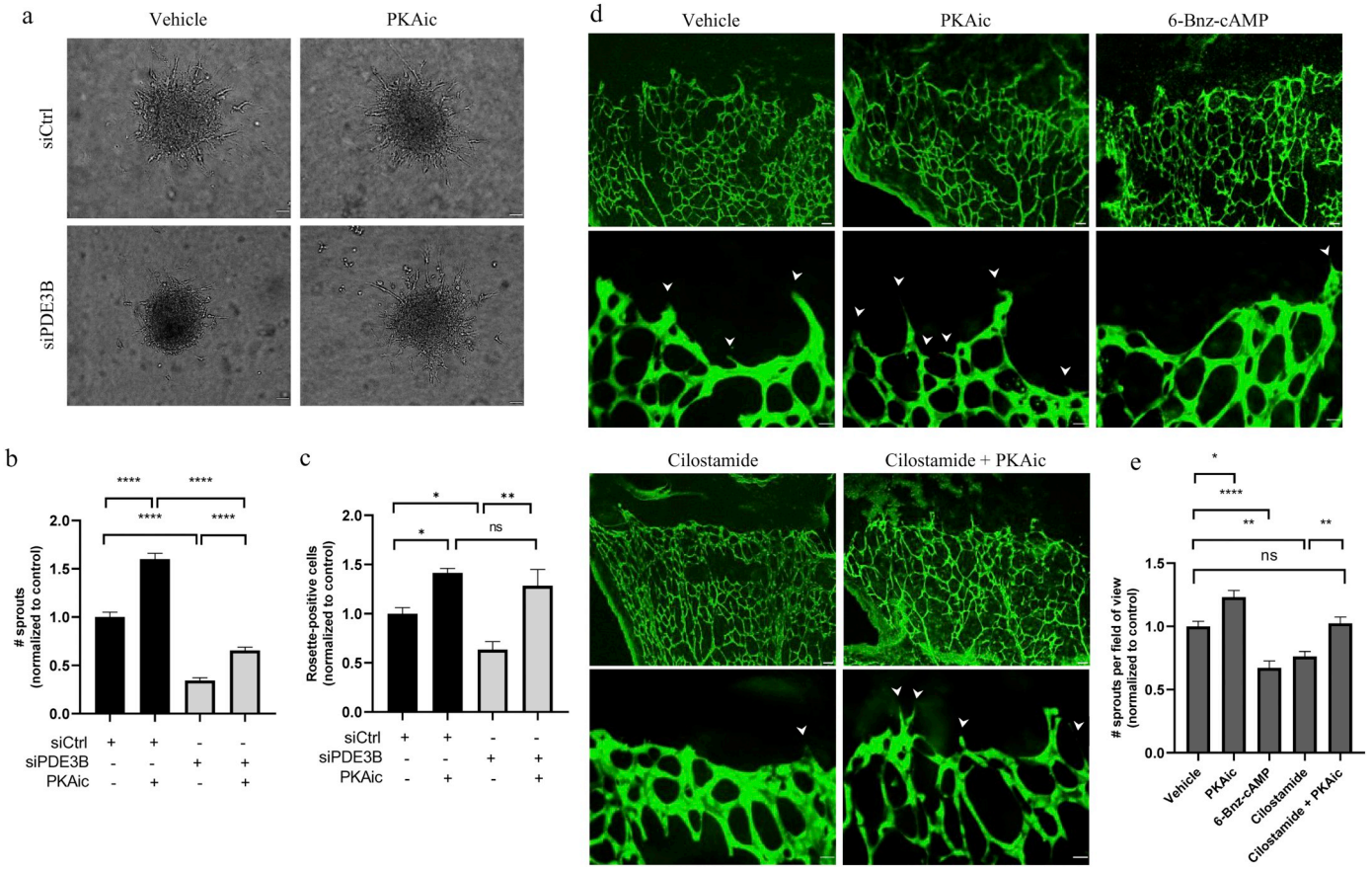

Fig. 4. Inhibition of PKA rescues the hypo-sprouting phenotype induced by PDE3B-knockdown *in vitro* and PDE3 inhibition *ex vivo*. (a) Representative brightfield images of control- and PDE3B-knockdown spheroids treated with PKAic or the vehicle; scale bars denote 50 μm. (b) Quantification of HAEC sprouting; ****p < 0.0001 in one-way ANOVA. (c) Quantification of the percent of control- and PDE3B-knockdown HAECs with podosome rosettes in the presence of PKAic or the vehicle; *p < 0.05, **p < 0.01 with one-way ANOVA. (d) Representative low and high magnification images of the sprouting front of an *ex vivo* mouse retinal model of angiogenesis. Retinas were isolated from postnatal day 5 mice and treated with PKAic ($n = 9$), 6-Bnz-cAMP (30 μM; $n = 7$), cilostamide (5 μM; $n = 10$), cilostamide + PKAic ($n = 8$), or the vehicle (n = 10). Angiogenic activity was evaluated by endothelial cell sprouting at the front of the vascular plexus (arrowheads). Scale bars in top panel denote 50 μm; scale bars in lower panel denote 25 μm. (e) Quantification of angiogenic sprouting in the *ex vivo* mouse retina model; *p < 0.05, **p < 0.01, ****p < 0.0001 in Kruskal-Wallis test.

of PDE3B. Remarkably, in the presence of PKA inhibitors, the percent of cells containing podosome rosettes was equivalent between control and PDE3B-knockdown HAECs (Fig. 4c). Collectively, these data indicate that a PDE3B-PKA signaling axis regulates the invasive functions of sprouting HAECs during angiogenic sprouting.

Upon identifying a regulatory role for the PDE3B-PKA complex during angiogenic sprouting *in vitro*, we next explored the role of PDE3B/PKA-signaling in the more physiologically relevant *ex vivo* retina model of angiogenesis. Consistent with our *in vitro* studies, PKA inhibition promoted angiogenic activity in the retina, measured as an increase in the number of sprouts at the front of the vascular plexus, while pharmacologic activation of PKA with 6-Bnz-cAMP impaired vascular sprouting (Fig. 4d, e). Interestingly, treatment of retinas with a PDE3 inhibitor significantly decreased sprouting at the vascular front, mirroring the effects of PKA activation (Fig. 4d, e). Importantly, when cilostamide and the PKA inhibitors were used in combination, PKA inhibition was sufficient to restore vascular sprouting relative to vehicle treated controls (Fig. 4d, e). Taken together, these data support the hypothesis that PDE3B activity regulates PKA-mediated control of angiogenic sprouting both *in vitro* and *ex vivo*.

3.4. The PDE3B-PKA complex acts upstream of cdc42 to regulate angiogenic sprouting

We previously reported that PKA negatively regulates angiogenic sprouting, at least in part, through its inhibition of cdc42 [18]. To explore the role of PDE3B in regulating cdc42-dependent sprouting, we first used an *in vitro* spheroid model of angiogenesis. Consistent with the hypothesis that PDE3B-PKA signaling acts upstream of cdc42, neither PKA inhibition nor PDE3 inhibition altered EC sprouting in cdc42-silenced HAEC spheroids (Fig. 5a, b). In addition, the impact of cdc42 inhibition on sprouting in PKA(Cα)-, PDE3B-, or control-knockdown spheroids further demonstrated that cdc42 acts downstream of each PKA and PDE3B. Thus, while treatment with the cdc42 inhibitor, ML141, significantly impaired angiogenic sprouting in control and PKA(Cα)-silenced HAEC spheroids, pharmacologic cdc42 inhibition had no effect on the sprouting function of PDE3B-knockdown spheroids (Fig. 5c, d), suggesting that the small RhoGTPase was maximally inhibited in cells with reduced levels of PDE3B. To confirm that PDE3B-PKA signaling indeed regulates cdc42 activity, we performed GST-PAK-PBD pulldown assays to evaluate the impact of PDE3B and/or PKA on the activation status of endogenous cdc42 in HAECs. In support of a role for this cAMP signaling system in regulating cdc42, treatment of HAECs with the PKA inhibitors significantly enhanced VEGF-induced cdc42 activation relative to vehicle-treated controls (Fig. 5e). In addition, in the presence of the PDE3 inhibitor, there was a trend toward a decrease in the level of active cdc42 following VEGF treatment (Fig. 5e).

Since our *in vitro* studies implicated a PDE3B-PKA-cdc42 signaling axis in the regulation of angiogenic sprouting, we next explored the dynamic regulatory functions of PDE3B, PKA and cdc42 in the *ex vivo*

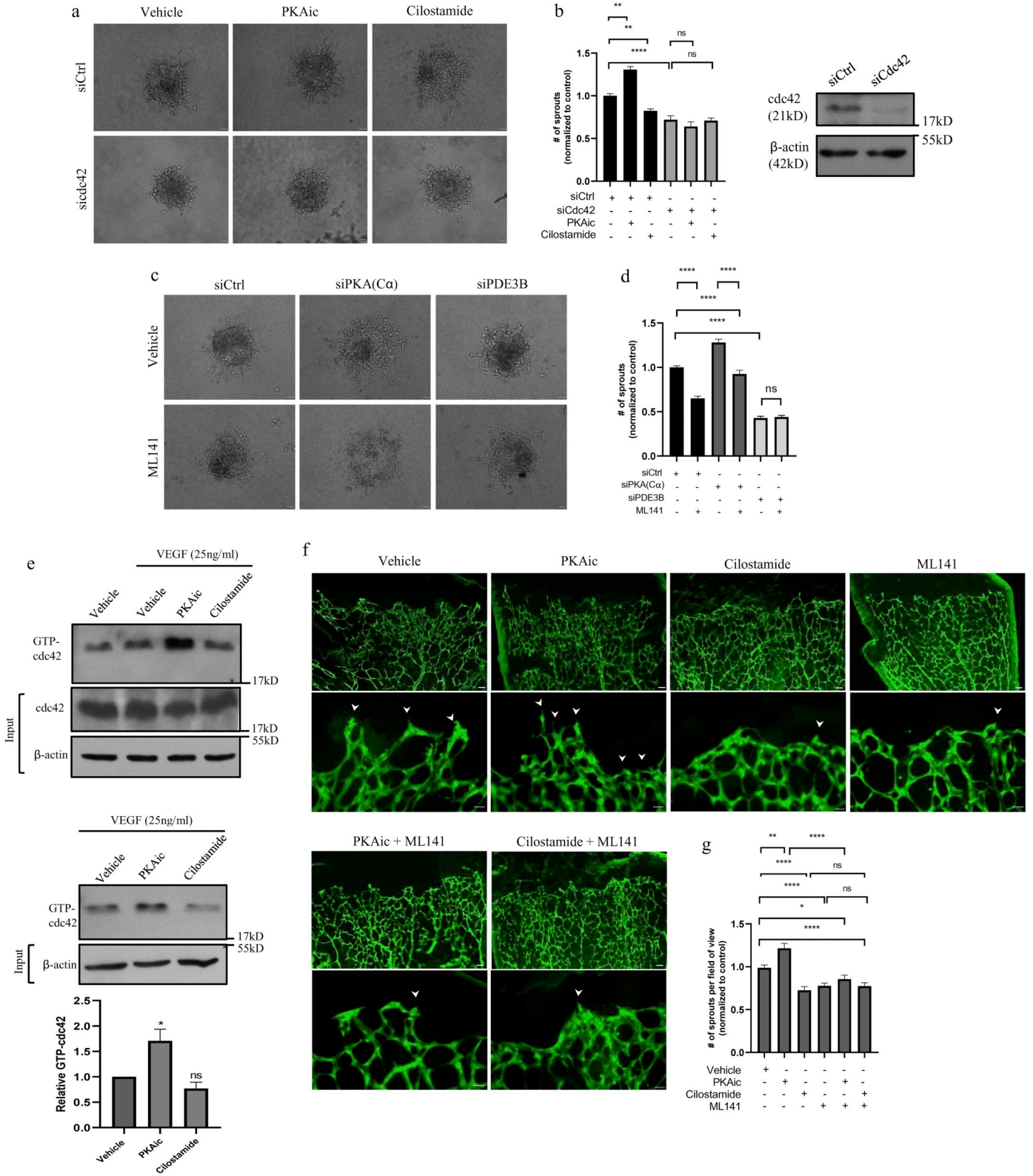

Fig. 5. The PDE3B-PKA signalosome regulates sprouting through the small RhoGTPase, cdc42. (a) Representative brightfield images of control and cdc42-knockdown HAECs spheroids in the presence of PKAic, cilostamide (5 μM), or the vehicle. Scale bars denote 50 μm. (b) Quantitation of HAEC sprouting (n = 3; **p < 0.01, ****p < 0.0001 in Kruskal-Wallis test) and accompanying cdc42 knockdown efficiency (***p < 0.001 in Student's unpaired t-test). (c) Representative brightfield images of control, PKA(Cα)-, and PDE3B-knockdown spheroids in the presence of ML141 (10 μM) or the vehicle. Scale bars, 50 μm. (d) Quantitation of HAEC sprouting; (n = 3; ****p < 0.0 in one-way ANOVA). (e) Representative immunoblots showing VEGF-induced cdc42 activation in the presence of PKAic, cilostamide (5 μM), or the vehicle; relative cdc42 activation is quantified for PKAic, cilostamide and vehicle treatments in the presence of VEGF (n = 3; *p < 0.05 in one-way ANOVA). (g) Representative low and high magnification images of the sprouting front of an *ex vivo* mouse retinal model of angiogenesis. Retinas were isolated from postnatal day 5 mice and treated with PKAic (n = 7), cilostamide (5 μM; n = 7), ML141 (10 μM; *n* = 12), PKAic + ML141 (n = 8), cilostamide + ML141 (n = 8), or the vehicle (n = 12). Scale bars in top panel denote 50 μm; scale bars in lower panel denote 25 μm. (h) Quantification of endothelial cell sprouting at the vascular front of the retina (*p < 0.05, **p < 0.01, ****p < 0.0001 in one-way ANOVA).

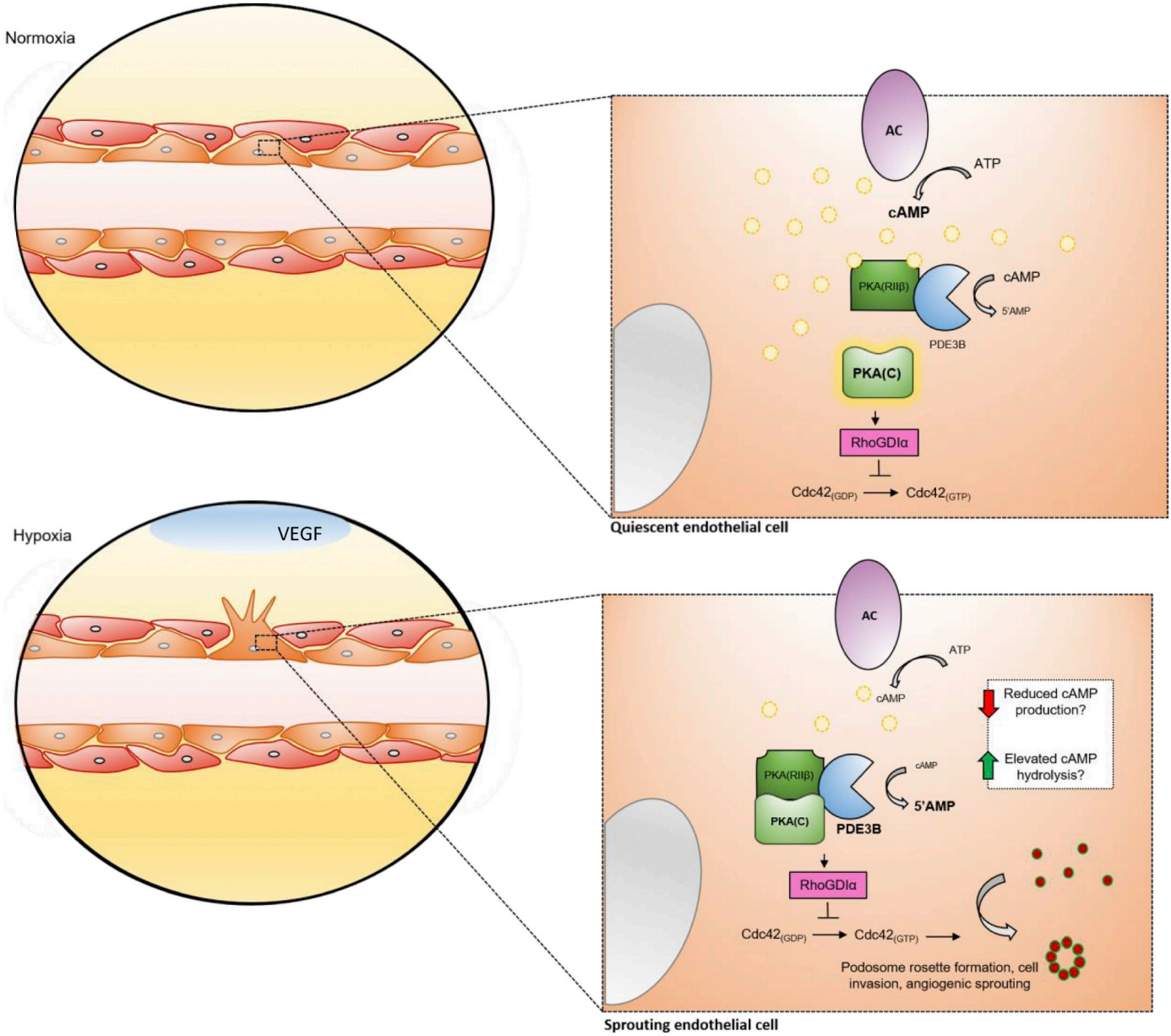

Fig. 6. Scheme depicting the PDE3B-PKA-cdc42 signaling axis and its influence on the angiogenic sprouting potential of ECs.

retina model of angiogenesis. In agreement with our cell-based studies, PKA inhibition induced a hyper-sprouting phenotype, while PDE3 and/or cdc42 inhibition reduced endothelial sprouting at the vascular front (Fig. 5g, h). Importantly, simultaneous inhibition of PKA and cdc42 obviated the pro-angiogenic effects of PKA inhibition (Fig. 5g, h), indicating that PKA acted upstream of cdc42 during vascular sprouting. Furthermore, when cilostamide and ML141 were used in combination, the effects of PDE3 inhibition and cdc42 inhibition were non-additive (Fig. 5g, h), suggesting that PDE3B and cdc42 regulate EC sprouting through a common signaling pathway. Taken together, these data support an intrinsic regulatory role for PDE3B-PKA signaling during cdc42-dependent sprouting (Fig. 6).

4. Discussion

Our work builds on previous reports that highlights an intrinsic inhibitory role for PKA during angiogenesis [17,18] by identifying PDE3B as the sole PDE responsible for regulating PKA activity in sprouting ECs. Thus, we show that PDE3, but not PDE2 or PDE4, activity regulates the "pool" of cAMP that allows PKA to antagonize EC sprouting. More specifically, we identify PDE3B as the unique PDE variant underpinning these effects, and present data consistent with the idea that PDE3B is afforded this role by virtue of its co-localization with PKA within a perinuclear cAMP-signaling compartment in these cells. Using *in vitro* and *ex vivo* models of angiogenesis, we demonstrate that PDE3 inhibition significantly impairs endothelial cell sprouting, mirroring the effects of pharmacologic PKA activation. Furthermore, our knockdown studies revealed an inverse regulation of angiogenic activity by PDE3B and PKA, as PDE3B-knockdown severely blunted EC sprouting, while reduced expression of PKA(Cα), or PKA inhibition, induced a hyper-sprouting EC phenotype. Importantly, PKA inhibition rescued vascular sprouting in both PDE3B-knockdown spheroids and retinal explants treated with the PDE3 inhibitor cilostamide, indicating that PDE3B regulates PKA activity during angiogenesis.

Examination of the individual cellular events required for EC sprouting provided insight into the mechanisms through which PDE3B controls this important process. Thus, while silencing PDE3B reduced the invasive capacity of HAECs by restricting podosome rosette

formation and matrix degradation, PKA inhibition reversed the effects of PDE3B-knockdown on podosome rosette biogenesis in these cells. Furthermore, inhibition of PKA partially restored angiogenic sprouting in PDE3B-silenced HAECs; these data are consistent with the observation that loss of PDE3B impairs both HAEC invasion and migration, while PKA only regulates the invasive function of ECs. Although further studies are required to elucidate the molecular mechanisms through which PDE3B regulates EC migration, previous work had identified a PDE3B-EPAC1 signalosome in HAECs [30,32], which may underpin the effects of this PDE on the migratory functions of these cells.

Several studies have reported a pivotal role for cdc42 in regulating EC angiogenic sprouting [33–35]. We previously reported that endothelial PKA restricts vascular sprouting, in large part, through its inhibition of cdc42 activity [18]. In agreement with these earlier findings, our current study largely supports a role for the PDE3B-PKA signaling in regulating cdc42-dependent sprouting. Using *in vitro* and *ex vivo* models of angiogenesis, we demonstrate that pharmacologic inhibition or RNAi-mediated silencing of cdc42 abolishes the effects of PKA and/or PDE3B on EC sprouting, indicating that both PDE3B and PKA act upstream of cdc42. In addition, we show that cdc42 inhibition impairs EC sprouting in both control and PKA(Cα)-knockdown HAECs, but that this treatment was without effect in cells with reduced levels of PDE3B. These data suggest that in the absence of PDE3B, PKA maximally inhibits cdc42 activity, and by extension, cdc42-dependent sprouting. While our previous work indicated that PKA inhibits cdc42 by promoting its interaction with the guanine nucleotide dissociation inhibitor (GDI), RhoGDIα [18], further studies are required to characterize the involvement of other GEFs, GAPs and GDIs and the roles of these regulators may play in further coordinating cdc42-dependent sprouting downstream of the PDE3B-PKA signaling identified here.

The integration of PDEs and cAMP effector proteins into highly localized cAMP signalosomes facilitates compartmentalized signaling and allows cAMP to control diverse functions selectively, and simultaneously, in cells [14,20]. Given that Nedvetsky and colleagues observed a hyper-sprouting phenotype in dnPKA^{iEC} mice, which express a dominant negative PRKARIα in ECs [17], we suspected that PDE3B might also interact with the PKARIα subunit in HAECs. Although our protein-protein interaction studies were not consistent with a strong interaction between PDE3B and PKARIα, they did confirm our previous reports which identified binding of endogenous PDE3B with PKARIIβ in HAECs [30]. Furthermore, immunostaining revealed co-localization of PDE3B and PKARIIβ within the perinuclear region of HAECs, while live cell imaging studies verified that PDE3B regulates a distinct perinuclear "pool" of PKA. Although this work illustrates that PDE3B is the cAMP-hydrolyzing enzyme that modulates the anti-angiogenic actions of PKA in ECs, further studies will be required to fully elucidate the signaling pathways involved in regulating PDE3B activity in response to pro-angiogenic agents. Given that previous work has characterized the activation of PDE3B by phosphoinositide-3-kinase (PI3K), protein kinase B (PKB) and PKA [36–41], current studies in our laboratory are aimed at addressing the post-translational regulatory mechanisms that may facilitate PDE3B activation during angiogenesis. In support of a critical role for PDE3B activity in normal angiogenic functioning, a recent study investigating endothelial dysfunction and impaired wound healing in type 2 diabetes described enhanced cAMP-PKA-CREB signaling as well as decreased expression of PDE3 in ECs isolated from diabetic animals [42], suggesting a potential link between dysregulated PDE3-PKA signaling and pathological angiogenesis.

Our data strongly suggest that reduced PKA activity facilitates EC sprouting. Given that the regulation of cAMP effector proteins is dependent upon the production and degradation of cAMP within distinct subcellular domains [20,21], a decrease in PKA activity during angiogenic sprouting would necessarily require enhanced cAMP hydrolysis and/or impaired cAMP production. While our work emphasizes a role for the cAMP-hydrolyzing PDE3B enzyme in regulating PKA activity, little is known regarding upstream signaling pathways that control cAMP production in response to pro-angiogenic stimuli. Recent studies have demonstrated that expression of C-X-C chemokine receptor type 4 (CXCR4), a Gαi-coupled GPCR, is upregulated in tip ECs during angiogenic sprouting and is essential for vessel development [11,43]. Since Gαi inhibits adenylyl cyclase, thus reducing cAMP production, endothelial CXCR4 may have a crucial, unexplored role in restricting downstream PKA activity that promotes angiogenic sprouting.

5. Conclusions

Here, we identify a novel PDE3B-PKA signaling complex in HAECs and provide mechanistic insight into cAMP-dependent regulation of angiogenic sprouting. Our works demonstrates that PDE3B has a crucial role in regulating PKA activity, which in turn restricts the intrinsic sprouting capacity of ECs *in vitro* and *ex vivo*. Protein interaction studies confirmed the direct interaction of PDE3B with PKARIIβ, while imaging studies revealed that this cAMP signalosome localizes within the perinuclear region of ECs. At a cellular level, we demonstrate that the PDE3B-PKA signalosome regulates angiogenic sprouting through its effects on invasive functions, including podosome rosette biogenesis and matrix degradation. At a molecular level, we show that PDE3B-PKA signaling regulates angiogenic sprouting, at least in part, through the small RhoGTPase, cdc42. Thus, this study identifies a novel role for PDE3B in regulating EC sprouting, which may represent a novel therapeutic strategy to target angiogenesis.

Conflict of interests

The authors declare that they have no conflict of interest.

Author contributions

J.L.M and D.H.M designed experiments; J.L.M performed a majority of the experiments and data analysis. P.B. performed and analyzed FRET experiments and real-time qRT-PCR. A.L.T. and M.L.O. provided transgenic mice. J.B.K. created AKAR-GR cell lines. J.L.M. and D.H.M. prepared the manuscript.

Acknowledgements

These studies were made possible through funds provided by the Canadian Institutes of Health Research (CIHR) to DHM (PJT 156283, Compartmented cAMP Signaling Regulates Human Arterial Endothelial Cell Inflammatory and Angiogenic Responses; MOP 57699, Vascular Endothelial Cell Activators and Shear Stresses in Health and Disease). JLM was funded through an Ontario Graduate Scholarship and the Robert John Wilson Fellowship. We would also like to thank Dr. Patricia Lima for assistance with confocal imaging, Melissa Mitchell and M. Bibiana Umana for technical assistance, and Dr. Stephen Archer for use of the Leica DMi8 inverted microscope.

References

[1] A.S. Chung, N. Ferrara, Developmental and pathological angiogenesis, Annu. Rev. Cell Dev. Biol. 27 (2011) 563–584, https://doi.org/10.1146/annurev-cellbio-092910-154002.
[2] H. Gerhardt, M. Golding, M. Fruttiger, C. Ruhrberg, A. Lundkvist, A. Abramsson, M. Jeltsch, C. Mitchell, K. Alitalo, D. Shima, C. Betsholtz, VEGF guides angiogenic sprouting utilizing endothelial tip cell filopodia, J. Cell Biol. 161 (2003) 1163–1177, https://doi.org/10.1083/jcb.200302047.
[3] R. Blanco, H. Gerhardt, VEGF and notch in tip and stalk cell selection, Cold Spring Harb. Perspect. Med. 3 (2013) a006569, https://doi.org/10.1101/cshperspect.a006569.
[4] H. Gerhardt, VEGF and endothelial guidance in angiogenic sprouting, Organogenesis 4 (2008) 241–246, https://doi.org/10.4161/org.4.4.7414.
[5] S.M. Weis, D.A. Cheresh, Tumor angiogenesis: molecular pathways and therapeutic targets, Nat. Med. 17 (2011) 1359–1370, https://doi.org/10.1038/nm.2537.
[6] L. Deveza, J. Choi, F. Yang, Therapeutic angiogenesis for treating cardiovascular diseases, Theranostics 2 (2012) 801–814, https://doi.org/10.7150/thno.4419.

[7] M. Potente, H. Gerhardt, P. Carmeliet, Basic and therapeutic aspects of angiogenesis, Cell 146 (2011) 873–887, https://doi.org/10.1016/j.cell.2011.08.039.

[8] Z. Szekanecz, A.E. Koch, Mechanisms of disease: angiogenesis in inflammatory diseases, Nat. Clin. Pract. Rheumatol. 3 (2007) 635–643, https://doi.org/10.1038/ncprheum0647.

[9] L. Jakobsson, C.A. Franco, K. Bentley, R.T. Collins, B. Ponsioen, I.M. Aspalter, I. Rosewell, M. Busse, G. Thurston, A. Medvinsky, S. Schulte-Merker, H. Gerhardt, Endothelial cells dynamically compete for the tip cell position during angiogenic sprouting, Nat. Cell Biol. 12 (2010) 943–953, https://doi.org/10.1038/ncb2103.

[10] M. Hellström, L.K. Phng, J.J. Hofmann, E. Wallgard, L. Coultas, P. Lindblom, J. Alva, A.K. Nilsson, L. Karlsson, N. Gaiano, K. Yoon, J. Rossant, M.L. Iruela-Arispe, M. Kalén, H. Gerhardt, C. Betsholtz, Dll4 signalling through Notch1 regulates formation of tip cells during angiogenesis, Nature 445 (2007) 776–780, https://doi.org/10.1038/nature05571.

[11] S.S. Hasan, R. Tsaryk, M. Lange, L. Wisniewski, J.C. Moore, N.D. Lawson, K. Wojciechowska, H. Schnittler, A.F. Siekmann, Endothelial notch signalling limits angiogenesis via control of artery formation, Nat. Cell Biol. 19 (2017), https://doi.org/10.1038/ncb3574.

[12] I.M. Aspalter, E. Gordon, A. Dubrac, A. Ragab, J. Narloch, P. Vizán, I. Geudens, R.T. Collins, C.A. Franco, C.L. Abrahams, G. Thurston, M. Fruttiger, I. Rosewell, A. Eichmann, H. Gerhardt, Alk1 and Alk5 inhibition by Nrp1 controls vascular sprouting downstream of notch, Nat. Commun. 6 (2015), https://doi.org/10.1038/ncomms8264.

[13] D.H. Maurice, Subcellular signaling in the endothelium: cyclic nucleotides take their place, Curr. Opin. Pharmacol. (2011) 656–664, https://doi.org/10.1016/j.coph.2011.10.009.

[14] A. Stangherlin, M. Zaccolo, Phosphodiesterases and subcellular compartmentalized cAMP signaling in the cardiovascular system, Am. J. Physiol. Circ. Physiol. 302 (2011) H379–H390, https://doi.org/10.1152/ajpheart.00766.2011.

[15] J. Surapisitchat, J.A. Beavo, Regulation of endothelial barrier function by cyclic nucleotides: the role of phosphodiesterases, Handb. Exp. Pharmacol. (2011) 193–210, https://doi.org/10.1007/978-3-642-17969-3_8.

[16] S.N. Rampersad, S.I. Freitag, F. Hubert, P. Brzezinska, N. Butler, M.B. Umana, A.R. Wudwud, D.H. Maurice, EPAC1 promotes adaptive responses in human arterial endothelial cells subjected to low levels of laminar fluid shear stress: implications in flow-related endothelial dysfunction, Cell. Signal. 28 (2016) 606–619, https://doi.org/10.1016/j.cellsig.2016.02.016.

[17] P.I. Nedvetsky, X. Zhao, T. Mathivet, I.M. Aspalter, F. Stanchi, R.J. Metzger, K.E. Mostov, H. Gerhardt, cAMP-dependent protein kinase a (PKA) regulates angiogenesis by modulating tip cell behavior in a notch-independent manner, Development. 143 (2016) 3582–3590, https://doi.org/10.1242/dev.134767.

[18] J.L. MacKeil, P. Brzezinska, J. Burke-Kleinman, A.W. Craig, C.J.B. Nicol, D.H. Maurice, A PKA/cdc42 signaling axis restricts angiogenic sprouting by regulating podosome rosette biogenesis and matrix remodeling, Sci. Rep. 20 (2019) 2385, https://doi.org/10.1038/s41598-018-37805-y.

[19] H. Jin, B. Garmy-Susini, C.J. Avraamides, K. Stoletov, R.L. Klemke, J.A. Varner, A PKA-Csk-pp60Src signaling pathway regulates the switch between endothelial cell invasion and cell-cell adhesion during vascular sprouting, Blood 116 (2010) 5773–5783, https://doi.org/10.1182/blood-2010-07-296210.

[20] D.H. Maurice, H. Ke, F. Ahmad, Y. Wang, J. Chung, V.C. Manganiello, Advances in targeting cyclic nucleotide phosphodiesterases, Nat. Rev. Drug Discov. 13 (2014) 290–314, https://doi.org/10.1038/nrd4228.

[21] M. Conti, D. Mika, W. Richter, Cyclic AMP compartments and signaling specificity: role of cyclic nucleotide phosphodiesterases, J. Gen. Physiol. 143 (2013) 29–38, https://doi.org/10.1085/jgp.201311083.

[22] A. Albini, R. Benelli, The chemoinvasion assay: a method to assess tumor and endothelial cell invasion and its modulation, Nat. Protoc. 2 (2007) 504–511, https://doi.org/10.1038/nprot.2006.466.

[23] G. Seano, G. Chiaverina, P.A. Gagliardi, L. Di Blasio, A. Puliafito, C. Bouvard, R. Sessa, G. Tarone, L. Sorokin, D. Helley, R.K. Jain, G. Serini, F. Bussolino, L. Primo, Endothelial podosome rosettes regulate vascular branching in tumour angiogenesis, Nat. Cell Biol. 16 (2014) 931–941, https://doi.org/10.1038/ncb3036.

[24] S.L. Kuo, C.L. Chen, Y.R. Pan, W.T. Chiu, H.C. Chen, Biogenesis of podosome rosettes through fission, Sci. Rep. 8 (2018) 524, , https://doi.org/10.1038/s41598-017-18861-2.

[25] L. Madisen, T.A. Zwingman, S.M. Sunkin, S.W. Oh, H.A. Zariwala, H. Gu, L.L. Ng, R.D. Palmiter, M.J. Hawrylycz, A.R. Jones, E.S. Lein, H. Zeng, A robust and high-throughput Cre reporting and characterization system for the whole mouse brain, Nat. Neurosci. 13 (2010) 133–140, https://doi.org/10.1038/nn.2467.

[26] S. Tual-Chalot, K.R. Allinson, M. Fruttiger, H.M. Arthur, Whole mount immunofluorescent staining of the neonatal mouse retina to investigate angiogenesis in vivo, J. Vis. Exp. 9 (2013) e50546, , https://doi.org/10.3791/50546.

[27] S.J. Netherton, D.H. Maurice, Vascular endothelial cell cyclic nucleotide phosphodiesterases and regulated cell migration: implications in angiogenesis, Mol. Pharmacol. 67 (2005) 263–272, https://doi.org/10.1124/mol.104.004853.

[28] T. Sudo, K. Tachibana, K. Toga, S. Tochizawa, Y. Inoue, Y. Kimura, H. Hidaka, Potent effects of novel anti-platelet aggregatory cilostamide analogues on recombinant cyclic nucleotide phosphodiesterase isozyme activity, Biochem. Pharmacol. 59 (2000) 347–356, https://doi.org/10.1016/S0006-2952(99)00346-9.

[29] C.M. Warren, M.L. Iruela-Arispe, Podosome rosettes precede vascular sprouts in tumour angiogenesis, Nat. Cell Biol. 16 (2014) 928–930, https://doi.org/10.1038/ncb3044.

[30] S.J. Netherton, J.A. Sutton, L.S. Wilson, R.L. Carter, D.H. Maurice, Both protein kinase a and exchange protein activated by cAMP coordinate adhesion of human vascular endothelial cells, Circ. Res. 101 (2007) 768–776, https://doi.org/10.1161/CIRCRESAHA.106.146159.

[31] Q. Ni, A. Ganesan, N.N. Aye-Han, X. Gao, M.D. Allen, A. Levchenko, J. Zhang, Signaling diversity of PKA achieved via a Ca2+ -cAMP-PKA oscillatory circuit, Nat. Chem. Biol. 7 (2011) 34–40, https://doi.org/10.1038/nchembio.478.

[32] L.S. Wilson, G.S. Baillie, L.M. Pritchard, B. Umana, A. Terrin, M. Zaccolo, M.D. Houslay, D.H. Maurice, A phosphodiesterase 3B-based signaling complex integrates exchange protein activated by cAMP 1 and phosphatidylinositol 3-kinase signals in human arterial endothelial cells, J. Biol. Chem. 286 (2011) 16285–16296, https://doi.org/10.1074/jbc.M110.217026.

[33] M. Xu, J. Lv, P. Wang, Y. Liao, Y. Li, W. Zhao, J. Zen, Z. Dong, Z. Guo, X. Bo, M. Liu, L. Zhang, G. Hu, Y. Chen, Vascular endothelial Cdc42 deficiency delays skin wound-healing processes by increasing IL-1β and TNF-α expression, Am. J. Transl. Res. 15 (2019) 257–268 (eCollection 2019).

[34] S. Suchting, C. Freitas, F. le Noble, R. Benedito, C. Breant, A. Duarte, A. Eichmann, The notch ligand Delta-like 4 negatively regulates endothelial tip cell formation and vessel branching, Proc. Natl. Acad. Sci. 104 (2007) 3225–3230, https://doi.org/10.1073/pnas.0611177104.

[35] B. Laviña, M. Castro, C. Niaudet, B. Cruys, A. Álvarez-Aznar, P. Carmeliet, K. Bentley, C. Brakebusch, C. Betsholtz, K. Gaengel, Defective endothelial cell migration in the absence of Cdc42 leads to capillary-venous malformations, Development 145 (2018) dev161182, , https://doi.org/10.1242/dev.161182.

[36] F. Ahmad, L.-N. Cong, L. Stenson Holst, L.-M. Wang, T. Rahn Landstrom, J.H. Pierce, M.J. Quon, E. Degerman, V.C. Manganiello, Cyclic nucleotide phosphodiesterase 3B is a downstream target of protein kinase B and may be involved in regulation of effects of protein kinase B on thymidine incorporation in FDCP2 cells, J. Immunol. 164 (2014) 4678–4688, https://doi.org/10.4049/jimmunol.164.9.4678.

[37] H.C. Young, S. Park, S. Hockman, E. Zmuda-Trzebiatowska, F. Svennelid, M. Haluzik, O. Gavrilova, F. Ahmad, L. Pepin, M. Napolitano, M. Taira, F. Sundler, L.S. Holst, E. Degerman, V.C. Manganiello, Alterations in regulation of energy homeostasis in cyclic nucleotide phosphodiesterase 3B-null mice, J. Clin. Invest. 116 (2006) 3240–3251, https://doi.org/10.1172/JCI24867.

[38] E. Degerman, F. Ahmad, Y.W. Chung, E. Guirguis, B. Omar, L. Stenson, V. Manganiello, From PDE3B to the regulation of energy homeostasis, Curr. Opin. Pharmacol. 11 (2011) 676–682, https://doi.org/10.1016/j.coph.2011.09.015.

[39] F. Ahmad, R. Lindh, Y. Tang, M. Weston, E. Degerman, V.C. Manganiello, Insulin-induced formation of macromolecular complexes involved in activation of cyclic nucleotide phosphodiesterase 3B (PDE3B) and its interaction with PKB, Biochem. J. 404 (2007) 257–268, https://doi.org/10.1042/bj20060960.

[40] R. Lindh, F. Ahmad, S. Resjö, P. James, J.S. Yang, H.M. Fales, V. Manganiello, E. Degerman, Multisite phosphorylation of adipocyte and hepatocyte phosphodiesterase 3B, Biochim. Biophys. Acta, Mol. Cell Res. 1773 (2007) 584–592, https://doi.org/10.1016/j.bbamcr.2007.01.010.

[41] D. Palmer, S.L. Jimmo, D.R. Raymond, L.S. Wilson, R.L. Carter, D.H. Maurice, Protein kinase a phosphorylation of human phosphodiesterase 3B promotes 14-3-3 protein binding and inhibits phosphatase-catalyzed inactivation, J. Biol. Chem. 282 (2007) 9411–9419, https://doi.org/10.1074/jbc.M606936200.

[42] M.S. Bitar, F. Al-Mulla, Upregulation of CREM/ICER suppresses wound endothelial CRE-HIF-1 -VEGF-dependent signaling and impairs angiogenesis in type 2 diabetes, Dis. Model. Mech. 8 (2014) 65–80, https://doi.org/10.1242/dmm.017145.

[43] M.E. Pitulescu, I. Schmidt, B.D. Giaimo, T. Antoine, F. Berkenfeld, F. Ferrante, H. Park, M. Ehling, D. Biljes, S.F. Rocha, U.H. Langen, M. Stehling, T. Nagasawa, N. Ferrara, T. Borggrefe, R.H. Adams, Dll4 and notch signalling couples sprouting angiogenesis and artery formation, Nat. Cell Biol. 19 (2017) 915–927, https://doi.org/10.1038/ncb3555.